Wake Integration for Three-Dimensional Flowfield Computations: Theoretical Development

Michael B. Giles*
Oxford University, Oxford OX1 3QD, England, United Kingdom
and
Russell M. Cummings†
California Polytechnic State University, San Luis Obispo, California 93407

This paper examines the analytical, experimental, and computational aspects of the determination of the drag acting on an aircraft in flight, with or without powered engines, for subsonic/transonic flow. Using a momentum balance approach, the drag is represented by an integral over a crossflow plane at an arbitrary distance behind the aircraft. Asymptotic evaluation of the integral shows the drag can be decomposed into three components corresponding to streamwise vorticity and variations in entropy and stagnation enthalpy. These are related to the established engineering concepts of induced drag, wave drag, profile drag, and engine power and efficiency. This decomposition of the components of drag is useful in formulating techniques for accurately evaluating drag using computational fluid dynamics calculations or experimental data.

Nomenclature

a	=	speed of sound
C	=	area of integration
c_p	=	specific heat at constant pressure
c_v	=	specific heat at constant volume
D	=	drag (force parallel to freestream direction)
E	=	rate of energy input as a result of fuel combustion
F	=	aerodynamic force vector
H	=	stagnation enthalpy
j, k	=	grid indexes
L	=	lift (force perpendicular to freestream direction)
n	=	surface normal unit vector
p	=	pressure
q	=	flow speed, $\equiv u^2 + v^2 + w^2$
R	=	universal gas constant
r	=	radius in polar coordinates
S	=	surface of integration
s	=	entropy
U_∞	=	freestream velocity vector
u	=	velocity vector
u, v, w	=	velocity components in x, y, z directions, respectively
x, y, z	=	Cartesian coordinate system
α	=	computational cell index; angle of attack
β	=	computational cell centroid
Γ	=	circulation
γ	=	vorticity
ζ	=	streamwise vorticity, distributed line source
θ	=	angle in polar coordinates
ρ	=	density
σ	=	crossflow function, $\equiv(\partial^2\phi/\partial y^2) + (\partial^2\phi/\partial z^2)$
τ	=	stress tensor
ϕ	=	velocity potential
ψ	=	stream function

Introduction

THE two most important aerodynamic quantities affecting an aircraft in flight are lift and drag. Nearly all aerodynamic analysis is an attempt to maximize the lift for a given amount of drag, or conversely to minimize the drag for a given amount of lift. The analysis of these quantities for various aircraft configurations forms the basis of most aerodynamic research. Because of this, reliable methods to compute these forces from available experimental or computational data are essential.

Traditionally, aerodynamic forces have been measured in wind tunnels using strain-gauge balances. This approach is very good for measuring the lift, but the drag of a typical aircraft at reasonable angles of incidence is often an order of magnitude less than the lift, and therefore, more difficult to measure. In particular, the presence of the model sting or support makes accurate drag measurement very difficult using this approach.

This led to attempts to measure drag using techniques based on a control volume approach. The simplest application of this is to measure the momentum deficit parallel to the freestream within the wake of a model. The main drawback to this approach, however, was the need to perform the wake survey throughout the downstream flowfield, as well as various difficulties associated with the presence of the wind-tunnel walls. An approach developed by Betz[1] modified the integral formulation to take into account the presence of the wind-tunnel walls, and reduced the area of integration to the region directly behind the model. Unfortunately, Betz did not include terms that would account for the drag resulting from vortices, an important aspect of measuring the drag of a finite span wing. His approach was also found to have certain measurement difficulties, as shown by Maull and Bearman.[2] In an attempt to correct some of the problems in Betz's approach, Maskell[3] showed that an integral formulation could be obtained that would allow the measurement of both profile and vortex drag, both of which could be obtained from measurements in a re-

duced region behind the aircraft. Since that time, various improvements to the Betz–Maskell model have been made for experimental measurements of drag.[4,5]

As computational fluid dynamics (CFD) has matured over the years, it has become a goal of CFD researchers to be able to predict aerodynamic drag from numerical simulations. Early attempts at doing this were usually met with frustration, as most approaches involved integrating the pressure and skin friction over the surface of the body to calculate forces (the computational equivalent of force measurement in the wind tunnel). Surface integration has met with difficulties because of the need to approximate the curved surface with flat facets, and the difficulty in accurately predicting the skin friction. This has led various researchers to attempt to apply the experimental wake integral methods to CFD computations. Methods involving wake integration have been shown to be reasonably accurate at predicting profile and vortex drag.[6,7] An equivalent lifting-line approach by Mathias et al.[8] has also been shown to be able to accurately compute induced drag.

The problem with the current approaches used to compute aerodynamic forces from CFD solutions is that various terms are usually neglected. These terms are known to be small far downstream of the aircraft, but in CFD calculations, the wake becomes increasingly diffuse downstream because of numerical smoothing, and so the integral methods need to be applied much closer to the aircraft. This paper looks carefully at the drag wake–survey methods, and comes to an improved understanding of the importance of the various integrals and the terms that are often neglected. The first approach is to take the crossflow plane to be far downstream of the aircraft, so that all flow components can be assumed to be approximately invariant in the freestream direction. This leads very simply to an integral form of the drag showing the different contributions caused by streamwise vorticity and variations in entropy and stagnation enthalpy. Next, an analysis is performed for a plane that is much closer to the aircraft, and at which there is still significant flow variation in the freestream direction. The same drag result is eventually obtained after careful analysis and appropriate asymptotic approximations. The purpose of this section is to relate the current analysis to the work of Refs. 1, 3, 4, 6, and 8–10. In practice, experimental measurement planes are always in this near-field region and there has been considerable discussion in the literature regarding the terms that should be included in the drag computation. It is shown in the analysis presented here that the terms resulting from the potential flow component of the velocity field cancel. A connection is also shown between the control volume formulation and the classical lifting-line theory of induced drag, showing that the current analysis reduces to the classical analysis under certain limiting conditions. The final sections discuss the application of the theory to the determination of drag from experimental measurements or computational results, including two analytic test cases.

Control Volume Formulation

The combined aerodynamic force, F, can be written as an integral over the surface of an aircraft as

$$F = \int_S (-p\mathbf{n} + \tau \cdot \mathbf{n})\, dS \qquad (1)$$

Using the integral form of the momentum equations, the force can also be expressed as an integral over the surface of any control volume enclosing the aircraft:

$$F = \int_S [-p\mathbf{n} - \rho(\mathbf{u}\cdot\mathbf{n})\mathbf{u} + \tau\cdot\mathbf{n}]\, dS \qquad (2)$$

If the far-field velocity relative to the aircraft is U_∞ aligned with the x-coordinate direction, then an equivalent form of the force integral is obtained using the conservation of mass:

$$F = \int_S [-(p - p_\infty)\mathbf{n} - \rho(\mathbf{u}\cdot\mathbf{n})(\mathbf{u} - U_\infty) + \tau\cdot\mathbf{n}]\, dS \qquad (3)$$

The control volume is now taken to be a cube aligned with the (x, y, z) coordinate axes, and with the downstream face a fixed distance downstream of the aircraft. As the size of the cube increases, the contribution to the drag component of the integral from the other five faces tends to zero. If the control volume surface is sufficiently far from the aircraft, the viscous stress terms may be neglected, and the final expression for the forces becomes

$$L = -\int\int \rho u w\, dy\, dz \qquad (4)$$

$$D = -\int\int [p - p_\infty + \rho u(u - U_\infty)]\, dy\, dz \qquad (5)$$

These equations are the common starting point for the development of methods of estimating the drag from experimental data.[11] It is interesting to note that Lighthill[11] preferred this formulation of the control volume integral for drag because the integrand only contains departures of flow quantities from their freestream values. This feature of the formulation may be very important when making force calculations using CFD solutions, where the far-field boundaries may not have freestream conditions. While the forces are often obtained directly by mounting the aircraft model on a sting and measuring the force using a balance, the drag is substantially smaller than the lift. This direct measurement of drag is more prone to measurement error, and so methods based on the control volume approach are often more accurate.

When using CFD methods, the aerodynamic forces on the aircraft can be evaluated by direct numerical approximation of the integral in Eq. (1), but even here there are benefits in using the drag integrals that result from the crossflow plane analysis. These include elimination of spurious drag because of numerical smoothing; potentially faster steady-state convergence of the drag estimate in time-marching computations, avoidance of possible errors because of far-field boundary conditions, and improved physical insight into the sources of drag for a particular aircraft configuration. These aspects are all discussed later in their relevant sections.

An additional integral that will be important for powered engines comes from the principle of energy conservation. If thermal diffusion and work resulting from viscous stresses are both negligible in the far field, then energy conservation over the control volume surface gives

$$E = \int_S \rho(\mathbf{u}\cdot\mathbf{n})\Delta H\, dS \qquad (6)$$

where $\Delta H = H - H_\infty$. Taking the control volume to be the same cube as before leads to the integral

$$E = \int\int \rho u \Delta H\, dy\, dz \qquad (7)$$

evaluated on the downstream crossflow plane.

Far-Field Analysis

Sufficiently far downstream of the aircraft, the flow is approximately invariant in the x direction. First, we consider a

flow in which there is no streamwise vorticity. In this case, the flow velocity is purely in the x direction:

$$u = [u(y, z), 0, 0] \tag{8}$$

and so, $p(y, z) = p_\infty$, to satisfy the y and z components of the momentum equations. Using the definitions of the stagnation enthalpy and entropy, with the freestream entropy defined to be zero, it follows that

$$\rho = \rho_\infty \exp(-s/c_p) \tag{9}$$

$$u = \{U_\infty^2 \exp(s/c_p) + 2[H - H_\infty \exp(s/c_p)]\}^{1/2} \tag{10}$$

These values can then be used to obtain the drag as

$$D = -\int\int \rho u(u - U_\infty)\, dy\, dz \tag{11}$$

If the entropy and perturbation in stagnation enthalpy are both small, then,

$$u \approx \left(U_\infty^2 + U_\infty^2 \frac{s}{c_p} + 2\Delta H - 2H_\infty \frac{s}{c_p}\right)^{1/2}$$

$$\approx U_\infty \left(1 + \frac{\Delta H}{U_\infty^2} - \frac{p_\infty}{\rho_\infty U_\infty^2} \frac{s}{R}\right) \tag{12}$$

and neglecting terms that are $\mathbb{O}[s^2, s\Delta H, (\Delta H)^2]$, Eq. (11) becomes

$$D \approx \int\int \left(p_\infty \frac{s}{R} - \rho_\infty \Delta H\right) dy\, dz \tag{13}$$

In inviscid flow without powered engines, ΔH is zero, and this reduces to the standard integral for transonic wave drag, first derived by Oswatitsch.[12] In viscous flow without powered engines, ΔH is usually still negligible. The increased entropy associated with the drag now comes from the shocks and dissipation in the boundary layer and wake, and so the drag integral is the combination of what is usually referred to as wave drag and profile drag. In the outflow from powered engines, ΔH is positive, corresponding to the work performed by the engine. The entropy will also be positive as a result of the inevitable thermodynamic cycle inefficiency and aerodynamic losses in the engine.

We now consider a flow with uniform entropy, stagnation enthalpy, and streamwise vorticity $\zeta(y, z)$. The velocity field now has the form

$$u = [U_\infty, v(y, z), w(y, z)] \tag{14}$$

To leading order, the density is uniform and mass is conserved. It is therefore possible to define the crossflow velocity components in terms of a crossflow stream function, which must satisfy the stream function/vorticity equation:

$$\nabla^2 \psi = -\zeta \tag{15}$$

When the entropy and stagnation enthalpy are both uniform, the pressure is related to the flow speed, yielding:

$$\Delta p \approx -\tfrac{1}{2}\rho_\infty(v^2 + w^2) \tag{16}$$

and the drag force is

$$D = \frac{1}{2}\rho_\infty \int\int (v^2 + w^2)\, dy\, dz \tag{17}$$

The simple physical interpretation of this equation is that the moving aircraft is doing work on the surrounding air at the rate DU_∞, which, in its wake, must equal the rate at which it is leaving kinetic energy associated with the crossflow.

It is possible to leave the integral in this form, but it is more convenient to express the velocity components in terms of the stream function and integrate by parts to obtain the following result, first obtained by Maskell[3]:

$$D = \frac{1}{2}\rho_\infty \int\int \psi\zeta\, dy\, dz \tag{18}$$

The lift integral [Eq. (4)], may also be simplified (see Ref. 13 for details of the development), resulting in:

$$L \approx \rho_\infty U_\infty \int\int y\zeta\, dy\, dz \tag{19}$$

There are many attractive features to these integrals: the vorticity is nonzero in only a limited area of the crossflow plane, so that the integration can be performed over a finite region; the values of these integrals are fairly insensitive to the streamwise location of the plane on which they are evaluated; and they clearly show the relationship between this component of drag and the shed vorticity associated with the lift on a finite span aircraft, the induced drag of the classic lifting-line theory. These relationships are further developed in a later section and in Ref. 13.

For a flowfield that has variations in the entropy and stagnation enthalpy in addition to streamwise vorticity, the two analyses can be approximately combined by adding the respective drag components, neglecting higher-order terms, to obtain

$$D \approx D_1 + D_2 + D_3 \tag{20}$$

where

$$D_1 = p_\infty \int\int \frac{s}{R}\, dy\, dz, \qquad D_2 = -\rho_\infty \int\int \Delta H\, dy\, dz$$

$$D_3 = \frac{1}{2}\rho_\infty \int\int \psi\zeta\, dy\, dz \tag{21}$$

This equation corresponds to the results in Ref. 10, if D_3 is kept in its crossflow kinetic energy form, as in Eq. (17).

In an experiment or computation, each of the three integrals will be a weak function of the streamwise position of the plane on which they are evaluated. While moving downstream, D_2 will approach a constant value, $-E/U_\infty$, where E is the rate of energy addition in the engines. D_3 will decay very slowly to zero as the streamwise vorticity diffuses, until the vorticity shed by one wing cancels the vorticity of the opposite sign shed by the other wing. In a CFD computation, because of numerical smoothing and coarse grids in the farfield, this will take place within the first 100 aircraft lengths; in reality it would take much longer. As D_3 decreases, there is a corresponding increase in D_1, because the total drag remains constant. In fact, the sum of the three components will be approximately constant well into the near field of the aircraft. This is fortunate because experimental measurements will usu-

ally have to be taken in the near field. Also, if a detailed breakdown of the sources of drag in a CFD calculation is required, it is best to evaluate the three integrals in the near field before numerical smoothing causes a shift from D_3 to D_1.

Near-Field Analysis

In the near field, in which there are significant variations in the x direction, the velocity field can be expressed using a Clebsch decomposition as

$$\boldsymbol{u} = \nabla\phi + \nabla \times \boldsymbol{\psi} \qquad (22)$$

where $\boldsymbol{\psi}$ is now a vector function, which satisfies the equation

$$\nabla^2\boldsymbol{\psi} = -\boldsymbol{\zeta} \qquad (23)$$

with $\boldsymbol{\zeta}$ being the vorticity vector. It is convenient to split $\boldsymbol{\psi}$ into the streamwise part $\psi\boldsymbol{i}$ and the remainder, so that

$$\boldsymbol{u} = \nabla\phi + \nabla \times (\psi\boldsymbol{i}) + \boldsymbol{u}_w \qquad (24)$$

The term $\boldsymbol{u}_w$ associated with the transverse vorticity is nonzero only in the wake. Its dominant component is in the streamwise direction, and so it corresponds to the velocity defect related to the variations in entropy and stagnation enthalpy, as discussed in the previous section. The link between transverse vorticity, entropy, and stagnation enthalpy is also explicit in Crocco's theorem for steady flow. The drag caused by this term can be written as a function of stagnation enthalpy and entropy variations, as before. Removing this term, we now concentrate on the drag associated with the velocity field.

Considering the pressure as a function of the flow speed, it was shown in Ref. 13 that

$$\frac{\mathrm{d}p}{\mathrm{d}(q^2)} = -\frac{1}{2}\rho \qquad (25)$$

Differentiating this term yields

$$\frac{\mathrm{d}^2p}{\mathrm{d}(q^2)^2} = -\frac{1}{2}\frac{\mathrm{d}\rho}{\mathrm{d}(q^2)} = -\frac{1}{2a^2}\frac{\mathrm{d}p}{\mathrm{d}(q^2)} = \frac{\rho}{4a^2} \qquad (26)$$

The change in freestream speed is

$$\Delta(q^2) = (U_\infty + \Delta u)^2 + v^2 + w^2 - U_\infty^2 \qquad (27)$$

and so performing a second-order Taylor series expansion about freestream conditions gives

$$\Delta p \approx -\tfrac{1}{2}\rho_\infty\Delta(q^2) + (\rho_\infty/8c_\infty^2)[\Delta(q^2)]^2$$
$$\approx -\tfrac{1}{2}\rho_\infty[v^2 + w^2 + 2U_\infty\Delta u + (1 - M_\infty^2)(\Delta u)^2] \qquad (28)$$

To first order, the corresponding change in density is

$$\Delta\rho \approx (\Delta p/a_\infty^2) \approx -(\rho_\infty U_\infty/a_\infty^2)\Delta u \qquad (29)$$

and so

$$\rho u\Delta u \approx \rho_\infty U_\infty\Delta u + \rho_\infty(\Delta u)^2 + \Delta\rho U_\infty\Delta u$$
$$\approx \rho_\infty U_\infty\Delta u + \rho_\infty(1 - M_\infty^2)(\Delta u)^2 \qquad (30)$$

Putting these into the drag integral, gives

$$D = \frac{1}{2}\rho_\infty\int\int [v^2 + w^2 - (1 - M_\infty^2)(\Delta u)^2]\,\mathrm{d}y\,\mathrm{d}z \qquad (31)$$

This equation corresponds to the results of Ref. 10, when there is no variation in entropy or stagnation enthalpy. Following

the approach of Maskell,[3] using a crossflow velocity potential, ϕ, and integrating by parts, gives

$$D = \frac{1}{2}\rho_\infty\int\int \psi\zeta\,\mathrm{d}y\,\mathrm{d}z - \frac{1}{2}\rho_\infty\int\int \phi\sigma\,\mathrm{d}y\,\mathrm{d}z$$
$$- \frac{1}{2}\rho_\infty\int\int (1 - M_\infty^2)(\Delta u)^2\,\mathrm{d}y\,\mathrm{d}z \qquad (32)$$

The first integral is exactly the same as what appeared in the far-field analysis. The second integral appears in the analyses of Maskell[3] and Wu et al.,[4] but is usually ignored in practice on the grounds that σ is small; this is essentially just the far-field argument used in the previous section. The third integral has been derived previously by Betz[1] for incompressible flow, and by Lock[9] and van der Vooren and Slooff[10] for compressible flow. Again, it is usually argued that this term is negligible.

In fact, to leading order, the second and third integrals cancel. To prove this requires the use of the mass equation which, to leading order, can be written as

$$U_\infty\frac{\partial\rho}{\partial x} + \rho_\infty\nabla\cdot\boldsymbol{u} = 0 \qquad (33)$$

From Eq. (29)

$$\frac{\partial\rho}{\partial x} \approx -\frac{\rho_\infty U_\infty}{a_\infty^2}\frac{\partial u}{\partial x} \qquad (34)$$

and so it follows that

$$(1 - M_\infty^2)\frac{\partial^2\phi}{\partial x^2} + \frac{\partial^2\phi}{\partial y^2} + \frac{\partial^2\phi}{\partial z^2} \approx 0 \qquad (35)$$

Hence, using integration by parts in both the y and z directions:

$$\frac{\mathrm{d}}{\mathrm{d}x}\int\int \phi\sigma\,\mathrm{d}y\,\mathrm{d}z = -\frac{\mathrm{d}}{\mathrm{d}x}\int\int (1 - M_\infty^2)\left(\frac{\partial\phi}{\partial x}\right)^2\,\mathrm{d}y\,\mathrm{d}z \qquad (36)$$

Integrating this ordinary differential equation in the x direction, with the boundary condition that both integrals tend to zero as $x \to \infty$, gives the final result that

$$\int\int \phi\sigma\,\mathrm{d}y\,\mathrm{d}z + \int\int (1 - M_\infty^2)(\Delta u)^2\,\mathrm{d}y\,\mathrm{d}z = 0 \qquad (37)$$

Thus, this analysis shows that it is correct to drop the potential flow term in Maskell's[3] analysis, and keep only the terms resulting from the trailing axial vorticity and the entropy and stagnation enthalpy variations, as derived in the previous section. This result should not be surprising: in the absence of any shed vorticity or variation in entropy or stagnation enthalpy, all flow quantities must approach freestream conditions in the farfield, and so there must be zero drag. As a consequence, the drag integral at any axial location in the near or far field must be identically zero.

Incompressible Flow

The drag expressions need to be modified if the numerical solution is obtained using an incompressible formulation, because variations in density and temperature may be negligible. To accommodate this case, the entropy is related to the stagnation pressure and enthalpy as

$$\frac{s}{R} \approx -\log\left(\frac{p_0}{p_{0_\infty}}\right) + \frac{\gamma}{\gamma - 1}\log\left(\frac{H}{H_\infty}\right) \approx -\frac{\Delta p_0}{p_{0_\infty}} + \frac{\gamma}{\gamma - 1}\frac{\Delta H}{H_\infty} \qquad (38)$$

Substituting this into the expression for the drag components D_1 and D_2, Eq. (21), yields

$$D_1 + D_2 \approx -\frac{p_\infty}{p_{0_\infty}} \int \int \Delta p_0 \, dy \, dz - \frac{1}{2} \rho_\infty U_\infty^2 \int \int \Delta H \, dy \, dz \tag{39}$$

For $M_\infty \rightarrow 0$, assuming no significant enthalpy variations, Eq. (39) becomes

$$D_1 + D_2 = -\int \int \Delta p_0 \, dy \, dz \tag{40}$$

which is the well-established result for incompressible flow.[11]

Connection to Lifting-Line Theory

In classical lifting-line theory, the wing is assumed to have a high aspect ratio and a flat sheet of streamwise vorticity shed behind it. The resulting drag caused by the shed vorticity is given by[14]

$$D = -\frac{\rho_\infty}{4\pi} \int_{-b/2}^{b/2} \int_{-b/2}^{b/2} \frac{\Gamma(y_0)\gamma(y)}{y_0 - y} \, dy \, dy_0 = \int_{-b/2}^{b/2} \gamma(y)f(y) \, dy \tag{41}$$

where

$$f(y) = -\frac{\rho_\infty}{4\pi} \int_{-b/2}^{b/2} \frac{\Gamma(y_0)}{y_0 - y} \, dy_0 \tag{42}$$

Now consider the drag component, D_3, in Eq. (21):

$$D = \frac{1}{2} \rho_\infty \int \int \psi\zeta \, dy \, dz \tag{43}$$

where the stream function satisfies Poisson's equation. The general solution to this equation, subject to the boundary condition that $\nabla\psi \rightarrow 0$ as $(y^2 + z^2) \rightarrow \infty$, is

$$\psi(y, z) = -\frac{1}{4\pi} \int \int \zeta(y_0, z_0)\log[(y - y_0)^2 + (z - z_0)^2] \, dy_0 \, dz_0 \tag{44}$$

where ζ represents a distributed line source of strength $\gamma(y)$ along $z_0 = 0$. The stream-function solution may be obtained by integrating by parts, using the fact that the circulation goes to zero at each wing tip, and taking the limit as $z \rightarrow 0$. The resulting relationship for the induced drag is (see Ref. 13 for details)

$$D = \int_{-b/2}^{b/2} \gamma(y)f(y) \, dy \tag{45}$$

which corresponds to the drag integral from lifting-line theory [Eq. (41)]. The lift per unit span is $\rho_\infty U_\infty \Gamma(y)$, and so the total lift is

$$L = \rho_\infty U_\infty \int_{-b/2}^{b/2} \Gamma(y) \, dy \tag{46}$$

Integrating by parts once gives

$$L = \rho_\infty U_\infty \int_{-b/2}^{b/2} y\gamma(y) \, dy \tag{47}$$

This corresponds precisely to the lift integral derived earlier for a general distribution of streamwise vorticity at the cross-flow plane [Eq. (19)], for the case where the vorticity is concentrated into a vortex sheet.

Thus, in the case of a planar vortex sheet, the stream-function–vorticity lift and drag integrals give the same result as classical lifting-line theory. The advantage of the stream-function–vorticity approach over the lifting-line theory is that it is much more general in its ability to handle nonplanar trailing streamwise vorticity, because of winglets, pylons, complex boundary-layer separations, etc. The advantage of the lifting-line theory is its extreme simplicity, and its ability to directly prove that an elliptic lift distribution minimizes the induced drag of a wing of fixed span and total lift.[8]

Experimental Applications

Experimental wake surveys have traditionally employed four- or five-hole probes from which the static pressure, stagnation pressure, and all three velocity components are obtained. Seven-hole probes are also being considered as a way to obtain these properties. The generally accepted method for computing induced drag based on such wake surveys is to compute the streamwise vorticity by differentiating the velocity field using

$$\zeta = \frac{\partial w}{\partial y} - \frac{\partial v}{\partial z} \tag{48}$$

This method of computing the streamwise vorticity can lead to errors in the prediction of the induced drag because of the differentiation of the discrete velocity measurements. One solution to this problem involves curve fitting the velocity field to obtain more accurate derivatives. An alternative approach is to relate the crossflow vorticity to the local circulation, and thus replace differentiation with integration.

For an arbitrary region, C, in a crossflow plane, the area integral of the streamwise vorticity is equal to the circulation around the boundary of C:

$$\int_C \zeta \, dy \, dz = \oint_{\partial C} (v \, dy + w \, dz) \tag{49}$$

Therefore, given the values of the crossflow velocity components, $v_{j,k}$ and $w_{j,k}$, at a uniform grid of measurement points in a crossflow plane (as shown in Fig. 1a), the streamwise component of vorticity in each measurement cell can be approximated by

$$\zeta_{j+1/2,k+1/2} = \Gamma_{j+1/2,k+1/2}/\Delta y \Delta z \tag{50}$$

where the circulation is defined by

$$\Gamma_{j+1/2,k+1/2} = \frac{1}{2}(v_{j,k} + v_{j+1,k})\Delta y + \frac{1}{2}(w_{j+1,k} + w_{j+1,k+1})\Delta z$$
$$- \frac{1}{2}(v_{j+1,k+1} + v_{j,k+1})\Delta y - \frac{1}{2}(w_{j,k+1} + w_{j,k})\Delta z \tag{51}$$

For an arbitrary distribution of vorticity, the stream function is

$$\psi(y, z) = -\frac{1}{4\pi} \int \int \zeta(y_0, z_0)\log[(y - y_0)^2 + (z - z_0)^2] \, dy_0 \, dz_0 \tag{52}$$
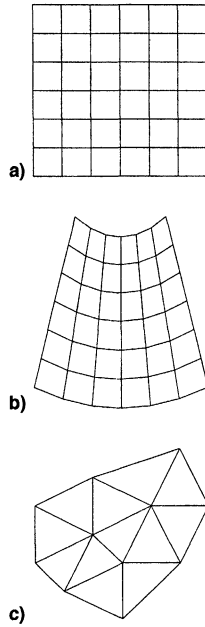
Fig. 1 Crossflow plane grids for the evaluation of drag integrals: a) Cartesian, b) unstructured, and c) structured.

Approximating the integral using the formulation first described by Lamb,[15] gives

$$\psi_{j,k} = -\frac{1}{4\pi} \sum_{j_0,k_0} \Delta y \Delta z \zeta_{j_0+1/2,k_0+1/2} \log \left[\left(j_0 + \frac{1}{2} - j \right)^2 \Delta y^2 \right.$$
$$\left. + \left(k_0 + \frac{1}{2} - k \right)^2 \Delta z^2 \right]$$

$$\psi_{j,k} = -\frac{1}{4\pi} \sum_{j_0,k_0} \Gamma_{j_0+1/2,k_0+1/2} \log \left[\left(j_0 + \frac{1}{2} - j \right)^2 \Delta y^2 \right.$$
$$\left. + \left(k_0 + \frac{1}{2} - k \right)^2 \Delta z^2 \right] \tag{53}$$

Finally, the drag integral can be approximated by summing over each cell to give the induced drag as

$$D = \frac{1}{2} \rho_\infty \sum_{j,k} \frac{1}{4} (\psi_{j,k} + \psi_{j+1,k} + \psi_{j,k+1} + \psi_{j+1,k+1}) \Gamma_{j+1/2,k+1/2} \tag{54}$$

In the absence of powered engines and any significant level of surface heat transfer, there is negligible variation in stagnation enthalpy. Therefore, the entropy can be deduced directly from the stagnation pressure and the corresponding drag integral is easily approximated.

In wind-tunnel experiments there is usually a sting supporting the model aircraft. Some CFD computations also model the sting to more accurately reproduce the experimental results and thereby deduce wind-tunnel corrections for the presence of the sting. Assuming that the sting is aligned with the freestream flow, the entire far-field control volume analysis can be repeated to include the presence of the sting. The drag components, D_1 and D_2 (resulting from entropy and enthalpy variations, respectively), are unchanged, apart from the fact that the integration is over the entire crossflow plane, except for the cross section of the sting. The only change to the induced drag integral, D_3, comes from the integration by parts, expressing the drag as a product of the stream function and vorticity:

$$D_3 = \rho_\infty \int\int (v^2 + w^2) \, dy \, dz = \rho_\infty \int\int \psi\zeta \, dy \, dz + \psi_s \Gamma_s \tag{55}$$

Here, Γ_s is the circulation around the sting, and ψ_s is the value of the stream function on the sting; for flows with symmetry about the plane $y = 0$, both of these are zero, but for flows with sideslip these terms may be nonzero.

The other complication is the presence of the sting in calculating the stream function associated with the vorticity. The simplest approach is to treat the sting as a region of flow with zero crossflow velocity. Thus, the surface of the sting becomes a vortex sheet, whose strength is equal to the tangential velocity of the flow around the sting. Equation (18) therefore remains valid if the contribution from the vortex sheet is included; the lift integral [Eq. (19)], is also unchanged if the vortex sheet contribution is included.

CFD Applications

For CFD calculations using unstructured grids, there is no crossflow plane in the computational grid, and so the most natural approach for the evaluation of the crossflow drag integrals is to adopt techniques from flow visualisation. A crossflow cutting plane can be defined orthogonal to the freestream flow and at a fixed distance downstream of the aircraft. The grid nodes on this cutting are defined by the intersection of the plane and the edges of the three-dimensional grid, and all flow variables can also be defined at the new grid nodes by linear interpolation along the cut edges. The nodes of the cutting planes are connected into triangles, based on the relationship of the cutting plane to the original cut cells. The full details for unstructured grids composed of tetrahedra, prisms, pyramids, and hexahedra are given by Giles and Haimes.[16] An example of the resulting unstructured triangular grid is shown in Fig. 1c.

Once the triangular cutting-plane grid has been constructed, the evaluation of the drag integral is quite straightforward. The circulation around a triangular cell is

$$\Gamma_\alpha = \sum_{\text{edges}} (\bar{v}\Delta y + \bar{w}\Delta z) \tag{56}$$

where $\bar{v}$ and $\bar{w}$ are the average velocity components on an edge, and Δy and Δz are the changes in y and z along the edge (going around the cell in a counterclockwise direction as viewed from $x = \infty$). The stream function at an arbitrary node is given by

$$\psi_j = -\frac{1}{4\pi} \sum_\beta \Gamma_\beta \log[(y_j - y_\beta)^2 + (z_j - z_\beta)^2] \tag{57}$$

where y_β, z_β are the coordinates of the centroid of the cell. The induced drag integral is then obtained from a summation over all of the triangular cells:

$$D = \frac{1}{2} \rho_\infty \sum_\alpha \bar{\psi}_\alpha \Gamma_\alpha \tag{58}$$

where $\bar{\psi}_\alpha$ is the average of the stream-function values at the three corner nodes.

Two refinements to the preceding formulation reduce the computational cost of evaluating the drag. The first addresses the problem that each stream-function value requires a loop over all of the cells in the crossflow plane. Therefore, the total computational cost is proportional to the square of the number of cells, which can be large for very fine grids. However, in general, only a few cells have significant levels of circulation, and it is only these cells that are needed for an accurate drag evaluation. Substituting Eq. (57) into Eq. (58) gives

$$D = \frac{1}{2} \rho_\infty \sum_{\alpha,\beta} \Gamma_\alpha \Gamma_\beta D_{\alpha\beta} \tag{59}$$

where

$$D_{\alpha\beta} = -\frac{1}{12\pi} \sum_j \log[(y_j - y_\beta)^2 + (z_j - z_\beta)^2] \quad (60)$$

with the j summation being over the three nodes at the corners of cell α. The drag summation [Eq. (59)] can be restricted to those values of α and β, for which the magnitudes of Γ_α and Γ_β exceed some minimum threshold. Setting a threshold can give a large reduction in the computational cost; detailed discussion of this concept are presented in Ref. 17.

The second refinement is for the common case in which the CFD computation is performed for a half-plane that is symmetric about $y = 0$. Rather than constructing the other half of the flowfield and then applying the preceding procedure, it is simpler to account for the image vorticity in defining the stream function as

$$\psi_j = -\frac{1}{4\pi} \sum_\beta \Gamma_\beta \{\log[(y_j - y_\beta)^2 + (z_j - z_\beta)^2]$$
$$- \log[(y_j + y_\beta)^2 + (z_j + z_\beta)^2]\} \quad (61)$$

For calculations on single- and multiblock-structured grids, it is unlikely that there exists a suitable grid coordinate plane that is at a uniform streamwise distance downstream of the aircraft. One option is to use the same cutting plane approach that was just presented, creating an unstructured triangular grid on the crossflow plane, with data interpolated along the cut edges of the structured grid. Further details about the application methods for CFD calculations can be found in Ref. 13.

The next issue is the interpretation of the values obtained from the drag integrals. Using CFD methods, it is possible to directly evaluate the aerodynamic force on the aircraft using a numerical approximation of the surface integral of Eq. (1). Almost all CFD methods are conservative, so that if the surface force integration is performed in a manner consistent with the CFD discretization of the cells with surface faces, then it is possible to sum over a very large number of computational cells surrounding the aircraft. Then it would be possible to deduce that the numerical surface force integral is exactly equal to that which would be obtained by a numerical force/momentum integral corresponding to Eq. (3), applied on the enclosing control surface. In the far field, numerical smoothing effects, such as the real viscous effects, are very small. Therefore, the far-field asymptotic analysis remains valid, showing that the numerical force integral on the aircraft surface can be equated to the drag integrals on the crossflow plane.

This raises the question of what is to be gained from evaluating the drag using the crossflow plane integrals rather than the direct surface integration. There are, in fact, four benefits in using the crossflow integrals:

1) In subsonic Euler calculations, the far field drag analysis shows two contributions. The one resulting from the streamwise vorticity, arising as a consequence of the spanwise lift distribution, is physically meaningful and should have very nearly the correct physical value because Euler calculations give relatively accurate lift predictions. The second contribution resulting from entropy variations is almost entirely spurious. Physically, there should be a slight level of entropy rise because of some early diffusion of the shed vorticity, but in the CFD computation almost all of the entropy will be a result of numerical smoothing in regions with high flow gradients and inadequate grid resolution, particularly near the leading edge of the wing. As a consequence, a more accurate prediction of the real aircraft drag is obtained by entirely neglecting the entropy drag integral, keeping only the induced drag streamwise vorticity integral. For transonic Euler calculations with shocks, and for Navier–Stokes calculations with entropy generation in the boundary layer, it is much harder to distin-

guish between physically correct entropy generation and spurious numerical generation, and so it may not be possible to apply such a correction.

2) If the boundaries are not sufficiently far from the aircraft, or if the boundary conditions are not sufficiently accurate, e.g., do not incorporate the far field correction caused by the lift on the aircraft, then there may be a very small error in the effective freestream flow angle. This will produce only a small error in lift, but can produce a more significant error in drag because the effective rotation of the lift vector means that the lift will contribute an apparent drag component of magnitude $L\Delta\alpha$. This problem is totally avoided by use of the downstream plane representation of the drag. The streamwise component of vorticity is only very slightly altered by a slight error in the freestream flow angle, and so the relative drag error will be extremely small.

3) When there are no powered engines, or when the stagnation enthalpy variation is sufficiently mixed so that it can be equated to the energy input to the engines, the drag depends solely on the entropy variations and the streamwise vorticity. These quantities change very little during the final stages of time-marching convergence to the steady-state solution. Therefore, the drag integral based on the downstream crossflow plane will converge to the final steady-state value quicker than the force integral over the surface of the aircraft. In practical CFD computations, this should allow fewer computational iterations to be required to obtain a given level of convergence of both the lift and drag.

4) Even if there were no quantitative advantages in expressing the drag in terms of the crossflow integrals, there is still a major qualitative benefit. Engineering analysis is simply one step in the process of engineering design: creating a better product. From this design viewpoint, it is important to not only know the value of overall drag, but to also understand the causes of the drag so that design decisions can be made to accomplish drag reduction. For example, a high level of induced drag for a given span and overall lift would suggest a poor spanwise lift distribution, which might be improved by changing the spanwise variation in the angle of attack or recambering certain parts of the wing. Alternatively, a large entropy drag might be caused by either poor wave drag because of shocks or poor profile drag because of a boundary-layer separation. This would therefore suggest areas of further study of the detailed CFD computation.

Evaluation of Drag Computations

Two test cases are used to validate the numerical discretization and programming implementation of the induced drag integral. The first is the wake behind an elliptically loaded planar wing. Using a unit semispan, the spanwise lift distribution is taken to be $\Gamma(\theta) = \sin\theta$, where the spanwise coordinate is $y = \cos\theta$ (see Fig. 2a). The crossflow velocity field in the wake is then given by

$$v(y, z) = -\frac{1}{2\pi} \int_0^\pi \frac{z}{(y - \cos\theta)^2 + z^2} \cos\theta \, d\theta \quad (62)$$

$$w(y, z) = \frac{1}{2\pi} \int_0^\pi \frac{y - \cos\theta}{(y - \cos\theta)^2 + z^2} \cos\theta \, d\theta \quad (63)$$

and the exact value for the drag is $\pi/8$, assuming unit freestream density.

Using a Cartesian grid of size 20×40 for the region $0 \le y \le 2$, $-1 \le z \le 1$, with clustering to accurately capture the vortex sheet and the large velocity gradients around the wing tip, as shown in Fig. 2b, the error from the numerical induced drag integral is only 1.1%. With a uniform Cartesian grid of the same size over the same region, as shown in Fig. 2c, the error increases to 15%, showing the effect of the decreased wake resolution.
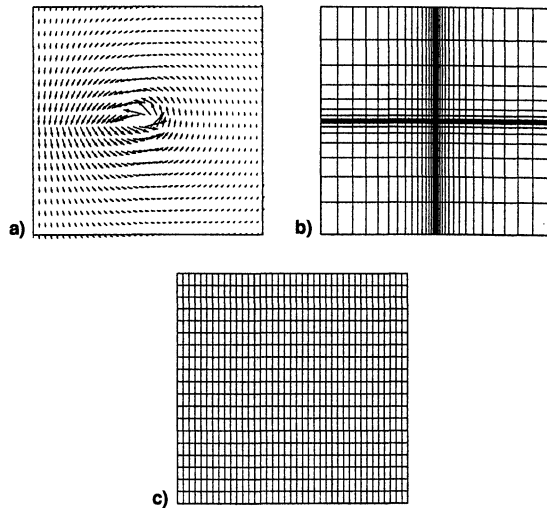
Fig. 2 Analytic test case no. 1: wake of an elliptically loaded planar wing: a) velocity vectors, b) stretched grid, and c) uniform grid.
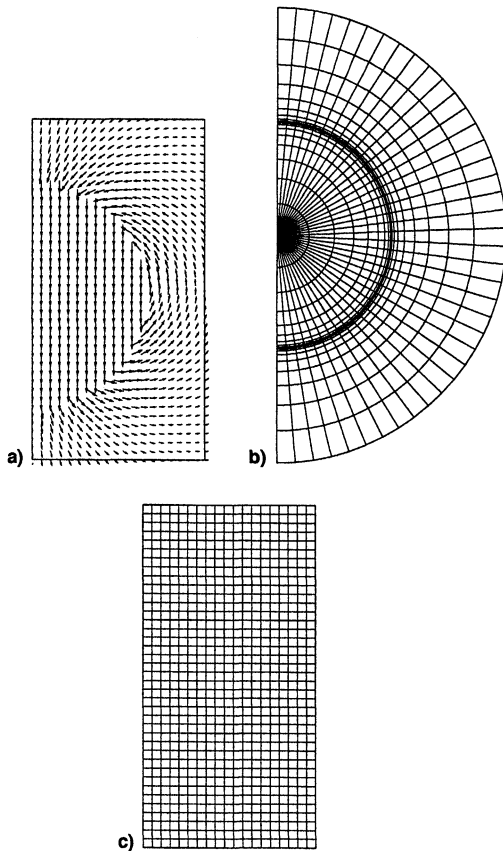

Fig. 3 Analytic test case no. 2: wake of a nonaligned engine: a) velocity vectors, b) stretched grid, and c) uniform grid.

The second case is the wake behind an engine, whose exhaust is not aligned with the freestream, as shown in Fig. 3a. Using polar coordinates, and assuming a unit radius for the engine, the crossflow velocity field is

$$v = \begin{cases} 0, & r < 1 \\ -\dfrac{\sin 2\theta}{r^2}, & r > 1 \end{cases}, \qquad w = \begin{cases} -1, & r < 1 \\ \dfrac{\cos 2\theta}{r^2}, & r > 1 \end{cases} \tag{64}$$

By integrating the crossflow kinetic energy, the exact value for the drag is found to be π, again assuming a unit freestream density.

Using a polar grid of size 20×40 for $0 \le r \le 2$, as shown in Fig. 3b, with clustering to accurately capture the vortex sheet at $r = 1$, the error from the numerical induced drag integral is only 1.4%. With a uniform Cartesian grid of the same size over the region $0 \le y \le 1.5$, $-1.5 \le z \le 1.5$ (see Fig. 3c), the error increases to 4.4%, again because of the effective smoothing of the velocity discontinuity across the vortex sheet.

Applications of these concepts to a variety of CFD solutions are performed in Ref. 17. The force integration method is applied to a variety of configurations, and the accuracy of the resulting drag calculations is related to various computational aspects, including grid type (structured or unstructured), grid density, flow regime (subsonic or transonic), boundary conditions, and the level of the governing equations (Euler or Navier–Stokes).

Conclusions

Analytical, experimental, and computational aspects of the determination of the forces acting on an aircraft in flight, with or without powered engines, for subsonic or transonic flow has been evaluated. Using a momentum balance approach, an integral over a crossflow plane at an arbitrary distance behind the aircraft is used to compute the lift and drag of an arbitrary aircraft configuration. Asymptotic evaluation of the integral shows that the drag can be decomposed into three components corresponding to streamwise vorticity and variations in entropy and stagnation enthalpy.

Terms in the near-field formulation that have previously been included in wake-integration formulas have been shown to cancel, leading to a unification of the near- and far-field formulations. The integrals are therefore related to the established engineering concepts of induced drag, wave drag, profile drag, and engine power and efficiency. The integrals are also shown to be equivalent to the results of lifting-line theory for a planar wing.

The decomposition of the components of drag is useful in formulating techniques for accurately evaluating drag using CFD calculations or experimental data. Suggestions have been made to improve the crossflow plane integration from discrete information by use of integration rather than differentiation. These suggestions apply to both computational and experimental applications. The crossflow plane evaluation of drag may prove to be highly useful in conjunction with numerical optimization schemes that are minimizing drag or maximizing lift-to-drag ratio.

Acknowledgments

References

[1]Betz, A., "Ein Verfahren zur Direkten Ermittlung des Profilwiderstandes," ZFM, Vol. 16, Feb. 1925, pp. 42–44.
[2]Maull, D. J., and Bearman, P. W., "The Measurement of the Drag of Bluff Bodies by the Wake Tranverse Method, Journal of the Royal Aeronautical Society, Vol. 68, Dec. 1964, p. 843.
[3]Maskell, E. C., "Progress Towards a Method for the Measurement of the Components of the Drag of a Wing of Finite Span," Royal Aircraft Establishment, TR 72232, Jan. 1973.
[4]Wu, J. C., Hackett, J. E., and Lilley, D. E., "A Generalized Wake-Integral Approach for Drag Determination in Three-Dimensional Flows," AIAA Paper 79-279, Jan. 1979.
[5]Brune, G. W., and Bogataj, P. W., "Induced Drag of a Simple Wing from Wake Measurements," Society of Automotive Engineers, TP 901934, Oct. 1990; also "Quantitative Low-Speed Wake Surveys," Journal of Aircraft, Vol. 31, No. 2, 1994, pp. 249–255.
[6]Van Dam, C. P., and Nikfetrat, K., "Accurate Prediction of Drag Using Euler Methods," Journal of Aircraft, Vol. 29, No. 3, 1992, pp. 516–519.
[7]Janus, J. M., and Chatterjee, A., "Use of a Wake-Integral Method for Computational Drag Analysis," AIAA Journal, Vol. 34, No. 1,

1996, pp. 188–190.

[8]Mathias, D. L., Ross, J. C., and Cummings, R. M., "Wake Integration to Predict Wing Span Loading from a Numerical Simulation," *Journal of Aircraft*, Vol. 32, No. 5, 1995, pp. 1165–1167.

[9]Lock, R. C., "Prediction of the Drag of Wings at Subsonic Speeds by Viscous/Inviscid Interaction Techniques," Royal Aircraft Establishment, TM Aero 2077, June 1986.

[10]Van der Vooren, J., and Slooff, J. W., "CFD-Based Drag Prediction: State-of-the-Art, Theory, Prospects," National Aerospace Lab., TP 90247, Aug. 1990.

[11]Lighthill, M. J., "Higher Approximation," *General Theory of High Speed Aerodynamics*, edited by W. R. Sears, Oxford Univ. Press, Oxford, England, UK, 1955, pp. 345–489.

[12]Oswatitsch, K., "Der Verdichtungsstoss bei der Stationären Umströmung Flacher Profile," *ZAMM*, Vol. 29, 1949, pp. 129–141.

[13]Cummings, R. M., Giles, M. B., and Shrinivas, G. N., "Analysis of the Elements of Drag in Three-Dimensional Viscous and Inviscid Flows," AIAA Paper 96-2482, June 1996.

[14]Anderson, J. D., *Fundamentals of Aerodynamics*, 2nd ed., McGraw–Hill, New York, 1991, pp. 324–330.

[15]Lamb, H., *Hydrodynamics*, 6th ed., Cambridge Univ. Press, Cambridge, England, UK, 1932, pp. 219, 220.

[16]Giles, M. B., and Haimes, R., "Advanced Interactive Visualization for CFD," *Computer Systems Engineering*, Vol. 1, No. 1, 1990, pp. 51–62.

[17]Hunt, D. L., Cummings, R. M., and Giles, M. B., "Wake Integration for Three-Dimensional Flowfield Computations: Applications," *Journal of Aircraft*, Vol. 36, No. 2, 1999, pp. 366–373.